Vietnam Journal of Earth Sciences, 48(1), 89–112, https://doi.org/ 10.15625/2615-9783/23833

Vietnam Journal of Earth Sciences
https://vjs.ac.vn/index.php/jse

Bias correction of CMIP6 rainfall projection for the Lake Toba region, Indonesia, using quantile delta mapping with monthly distribution fitting

Syukri Arif Rafhida, Sri Nurdiati*, Retno Budiarti, Mohamad Khoirun Najib

School of Data Science, Mathematics, and Informatics, IPB University, Bogor, Indonesia

Received 30 May 2025; Received in revised form 14 October 2025; Accepted 25 November 2025

ABSTRACT

Accurate climate projections are crucial for water resource management in the Lake Toba region of Indonesia, where rainfall supports agriculture, tourism, and hydropower. However, rainfall projections from CMIP6 global climate models (GCMs) often exhibit systematic biases due to coarse spatial resolution and model assumptions. This study applies the statistical bias-correction method, Quantile Delta Mapping (QDM), to adjust CMIP6 rainfall outputs using observed data from seven weather stations around Lake Toba. The study employs ten probability distributions and compares two distribution identification approaches: monthly and full-period. Results show that monthly distribution identification (QDM1) improves model performance more consistently, reducing the Kolmogorov-Smirnov (KS) error by the raw CMIP6 data by 47.26% compared to 20.39% from the full-period approach (QDM2). Post-correction projections using a Multi-Model Ensemble Mean (MMEM) for 2015–2050 under scenarios SSP2-4.5 and SSP5-8.5 indicate moderated rainfall trends in 2050 after correction, notably reduced overestimation in wet seasons. These more conservative projections suggest slight decreases during MAM, contrasting with the uncorrected CMIP6 tendency toward wetter futures. It also suggests the future use of regional climate models (RCMs) and nonparametric or machine-learning methods to capture more complex rainfall distribution patterns in the region.

Keywords: Bias correction, CMIP6, equatorial climate, Lake Toba, Quantile Delta Mapping, rainfall.

1. Introduction

Lake Toba, the largest volcanic and tectonic lake in Indonesia (Chesner, 2012), has an equatorial climate characterized by two rainy seasons and two dry seasons, resulting in year-round rainfall (Aldrian and Susanto, 2003; Hermawan, 2010; Nurdiati et al., 2021). This rainfall supports key sectors such as agriculture, food security, tourism, and the supply of water and electricity for surrounding communities (Sihotang et al., 2012). However, the threat of climate change is expected to increase the uncertainty of rainfall patterns around Lake Toba (Irwandi et al., 2023). This uncertainty may stem from various factors, such as ENSO and IOD (Nurdiati et al., 2024, 2022). Irwandi et al. (2017) reported a decrease in rainfall in the Lake Toba area in 2016 due to climate anomalies. This situation highlights the critical importance of rainfall forecasting for communities around Lake Toba to take necessary preventive measures in response to potential climate change impacts.

---

*Corresponding author , Email: nurdiati@apps.ipb.ac.id

Currently, global climate models (GCMs), such as those developed under the Coupled Model Intercomparison Project (CMIP), are the primary tools for simulating current climate conditions and projecting future climate change. (Chen et al., 2013; Eyring et al., 2016). CMIP6, the latest advancement from CMIP5 (Grose et al., 2020), uses the Shared Socioeconomic Pathways (SSPs), which are climate change scenarios designed to explore how socioeconomic factors might influence future climate changes. These factors include population, economic growth, education, urbanization, and technological development (Riahi et al., 2017). Among these, three scenarios are commonly used: a mitigation-focused scenario (SSP1-2.6), a medium scenario (SSP2-4.5), and a high-emissions scenario without mitigation (SSP5-8.5) (Noël et al., 2021).

In recent years, GCMs have improved in their ability to predict rainfall with higher resolution and greater accuracy. (Karmalkar et al., 2019). However, they still operate at relatively coarse spatial resolutions. (100–250 km), making them less suitable for regional climate studies (Ahn et al., 2016; Salathé, 2003; Schoof and Robeson, 2016), such as those focused on Lake Toba. The coarse resolution of GCMs limits their ability to provide outputs that can be used directly to assess regional climate change impacts. (Schoof, 2015). Additionally, GCMs are subject to systematic errors, or biases, when compared with observed data. (Ho et al., 2012). To overcome these limitations, downscaling and bias correction methods are essential. These methods allow GCM outputs to be adjusted using local climate data from local weather stations, such as those provided by Badan Meteorologi, Klimatologi, dan Geofisika (BMKG). By applying bias correction to BMKG station data, GCM outputs can become more accurate and relevant for assessing localized climate impacts.

Various bias-correction methods have been developed to minimize bias in climate models. One of the most widely used methods involves correcting the probability distributions of simulated variables by applying adjustment factors to the cumulative distribution functions (CDFs) of both modeled and observed data. An example of such a method is quantile mapping (QM), which is based on empirical CDFs (Li and Li, 2023). QM is considered advantageous because it can correct biases in the mean and standard deviation, and even in extreme events (Teutschbein and Seibert, 2012). However, a key limitation of QM is its reliance on a stationary statistical relationship between historical and future periods. When future values fall outside the reference range, QM can extrapolate poorly, leading to over- or underestimation and skewed distributions. In addition, conventional QM may distort the underlying climate-change signal. This highlights the need for methods that can more effectively preserve these signals, such as quantile delta mapping (QDM). Quantile delta mapping (QDM), developed from QM, retains QM's strengths while accounting for changes in the CDF across different time periods. QDM's key advantage lies in its ability to preserve the trend in climate model outputs, an essential feature for climate change analysis (Cannon, 2018).

Many studies have adopted QDM as a bias-correction tool in their research (Rafhida et al., 2024; Reboita et al., 2023). While Cannon et al. (2015) used only the gamma distribution in their QDM implementation, different climate data distributions may exhibit varying skewness and symmetry. Irwandi et al. (2023) used other distributions to model rainfall and temperature, including the generalized extreme value, Normal, Weibull, Gamma, logistic, Lognormal, Log-logistic, and Inverse Gaussian distributions. Ten distributions were also used by, who included the extreme value and exponential distributions to identify sea surface temperature distributions, revealing that distribution types vary by location.

The study by Irwandi et al. (2023) also highlighted that distributions vary not only across locations but also from month to month. This insight has led to the development of new approaches to QDM, which involve not only full-period corrections but also month-by-month corrections. In equatorial, low-interannual-variability settings like Lake Toba, month-wise QDM will outperform full-period fitting because it avoids mixing wet- and dry-season regimes. Rafhida et al. (2024) found that both correction methods are effective depending on the local rainfall patterns in different parts of the Lake Toba region This creates an urgent need to apply bias correction to CMIP6 global climate data using BMKG station data to improve climate models for Lake Toba using QDM, incorporating multiple correction methods. Therefore, this study focuses on applying QDM-based bias correction to CMIP6 climate data around Lake Toba using 10 probability distributions and 2 distribution-identification approaches. It also aims to provide rainfall projections for the Lake Toba region based on bias-corrected CMIP6 global climate models. Through this study, we strive to improve rainfall climate modeling, which is of significant importance to the communities and ecosystems surrounding the lake.

2. Study Area and Data

Lake Toba, located in North Sumatra Province, Indonesia, spans across seven regencies: Karo, Simalungun, Dairi, Toba Samosir, Samosir, North Tapanuli, and Humbang Hasundutan. Geographically, it lies between 98°31'2"–98°9'14" East Longitude and 2°19'15"–2°54'2" North Latitude (Fig. 1). The lake covers a surface area of 1,124 km², with an approximate length of 50 km, a width of 27 km, and an average depth of 228 meters (Lukman, 2010).

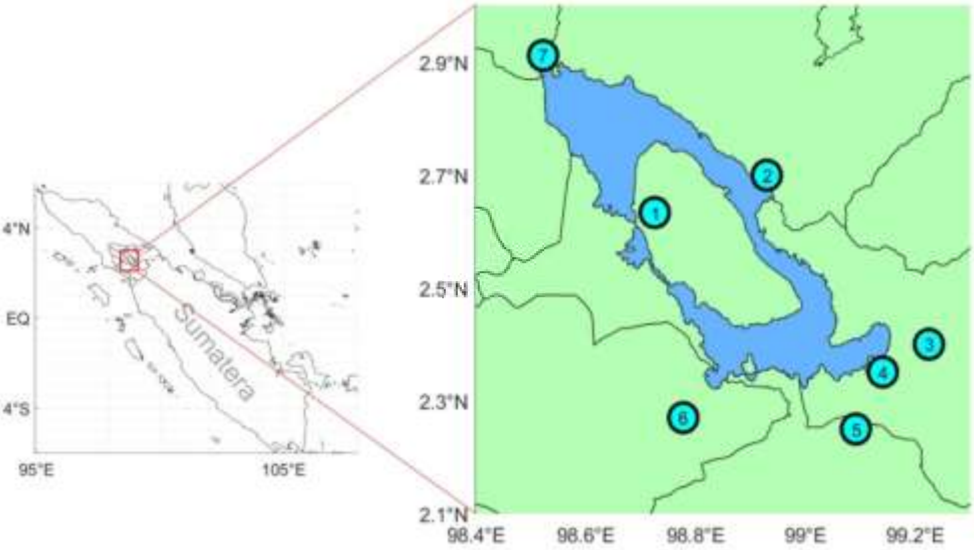

Figure 1. Location of the Toba Lake, and observation station in Lake Toba area

Lake Toba is situated in an equatorial climate zone, characterized by a bimodal rainfall pattern with two primary peaks occurring between March and May and October-November (Aldrian & Susanto, 2003). This pattern is primarily influenced by the migration of the Intertropical Convergence Zone (ITCZ), which shifts north and south due to the apparent annual motion of the sun (Tukidi, 2010). The ITCZ movement enhances convection and cloud formation in the equatorial region, resulting in relatively high rainfall throughout the year compared to monsoonal or semi-arid regions.

Aldrian and Susanto (2003) observed that regions with equatorial climates tend to receive higher monthly rainfall than those with other climate types, with average monthly rainfall exceeding 150 mm and peak values reaching approximately 310 mm during October–November. In contrast, monsoonal regions exhibit more varied rainfall patterns, with lower dry season rainfall averaging around 100 mm per month. (Fig. 2) illustrates the annual rainfall cycle over Lake Toba, derived from the average of seven BMKG rain-gauge stations (Fig. 2a) and the general equatorial climate (Fig. 2b).

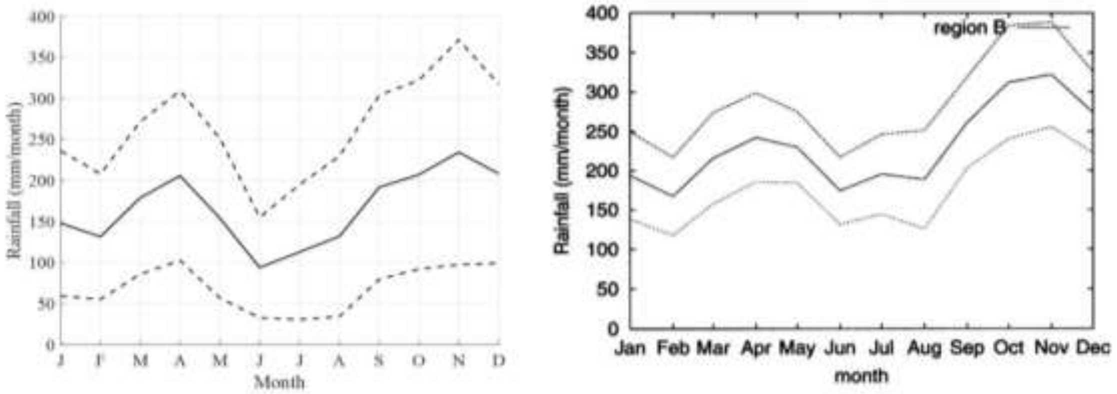

(a) (b)

Figure 2. Annual cycle of monthly total rainfall (a) Lake Toba and (b) equatorial climate zones (Aldrian and Susanto, 2003). Solid lines represent the mean, while dashed lines represent the standard deviation

Overall, the average monthly rainfall in Lake Toba is approximately 50 mm/month lower than the average rainfall in previously studied equatorial regions in 2003. This discrepancy may be due to several factors. Previous research by Irwandi et al. (2023) reported that rainfall in the Lake Toba area has decreased due to climate change, highlighting the importance of continuous and reliable rainfall observations for understanding potential future extreme weather events. In Indonesia, rainfall data recorded by the Badan Meteorologi, Klimatologi, dan Geofisika (BMKG) follow standardized procedures widely used in climate research, ensuring data consistency and reliability. However, as noted by Mamenun et al. (2014) Incomplete or unevenly distributed rainfall records may still occur due to manual data entry or instrument malfunctions. Such limitations can affect temporal consistency, underscoring the importance of accurate rainfall forecasting for local communities around Lake Toba to prepare preventive measures against potential extreme weather events.

Additionally, the topography of Lake Toba surrounded by hills and the Bukit Barisan mountain range can influence rainfall distribution through the rain shadow effect. This is consistent with the findings of Prasetyo et al. (2018), who noted that Lake Toba, located in a mountainous area, receives less rainfall than the western part of North Sumatra. The Barisan Mountains, stretching along the west coast of Sumatra, act as a major barrier to moisture-bearing winds from the Indian Ocean.

The data used in this study consists of both observational and model data. Observational data were obtained from BMKG North Sumatra, comprising monthly total rainfall from 1973 to 2014 at seven stations surrounding Lake Toba. Thus, the observational dataset has a shape of 540 × 7, representing 540 months of rainfall across seven stations. As shown in Fig. 1, the observational data locations around Lake Toba include, in order from 1 to 7: Pangururan, Parapat, Silaen, Laguboti, Siborong-borong, Doloksanggul, and Merek.

The model data consist of CMIP6 data retrieved from https://cds-beta.climate.copernicus.eu/datasets/projections-cmip6 in netCDF format; the specific CMIP6 models employed in this study are listed in Table 1, following Mareta et al. (2024). In line with their Sumatra-wide screening, we prioritize models with finer native grids (≈ ≤1.5°) and documented performance for tropical precipitation, retaining EC-Earth3-Veg-LR, CNRM-CM6-1, MRI-ESM2-0, and BCC-CSM2-MR while excluding very coarse configurations (e.g., CanESM5 at ~2.8°) that under-resolve the orographic and coastal controls around Lake Toba.

Table 1. List of CMIP6 models used in the study

Models	**Abbreviation**	**Instituion**	**Resolution**	**Reference**
BCC-CSM2-MR	BCC	China	1.12° × 1.12°	(Wu et al., 2018)
EC-Earth3-Veg-LR	EC	Europe	1.12° × 1.12°	(Döscher et al., 2022)
CNRM-CM6-1	CNRM	France	1.4° × 1.4°	(Voldoire, 2018)
MRI-ESM2-0	MRI	Japan	1.12°× 1.12°	(Yukimoto et al., 2019)

CMIP6 includes two time periods: a historical period and a projection period. The historical period covers 1950 to 2014. Typically, CMIP6-based studies divide the projection period into three parts: near future (2015–2040), mid future (2041–2070), and far future (2071–2100) (Supharatid et al., 2022). However, other studies, such as that by Schroeter et al. (2024), define the near future as extending to 2050, offering a broader temporal scope for assessing medium-term climate change impacts. In line with this approach, this study uses the near future period (2015–2050).

CMIP6 also introduced the Shared Socioeconomic Pathways (SSPs), which enable climate projections based on different future socioeconomic trajectories. These factors include population growth, economic development, education, urbanization, and technological advancement. Three of the commonly used SSP scenarios are: a mitigation scenario (SSP1-2.6), a medium pathway (SSP2-4.5), and a no-mitigation pathway (SSP5-8.5) (Mishra, Bhatia & Tiwari, 2020). This study uses SSP2-4.5 and SSP5-8.5. Table 1 below shows the spatial resolution of each CMIP6 model used by Mareta et al. (2024) in their study of Sumatra Island, with resolutions less than 2°.

3. Methods

3.1. Data Extraction

The climate model data includes three variables: longitude, latitude, and precipitation (denoted as pr). The unit of the precipitation variable is kg m^2 s^{-1}. We convert it to monthly rainfall (mm/month). The baseline data used for bias correction is the historical period (1973–2014), which is divided into a calibration period (k) (1973–2003) and a validation period (v) (2004–2014). The observed calibration data is denoted as $x_{o,k}$ and the model calibration data as $x_{m,k}$. Similarly, the model and observation data for the validation period are labeled as $x_{m,v}$ and $x_{o,v}$ Respectively. The model projection data is denoted as $x_{m,p}$.

Interpolation is applied to adjust CMIP6 model data to the exact locations of BMKG weather stations. The model data have a coarse spatial resolution (see Table 1), typically 1–2°, while the observation stations are located at a finer resolution of 0.001 × 0.001°. For instance, the Pangururan station is situated at 2.633°N, 98.726°E. Therefore, bicubic spline interpolation is used to estimate model rainfall at each of the seven observation stations. While any interpolation from coarse grids to point locations can introduce additional errors, such as smoothing of extremes and representativeness mismatch due to scale differences (Hofstra et al., 2010). We adopt bicubic because it provides smooth, continuous gradients (C^1 continuity) and reduces blocky artifacts relative to linear or nearest-neighbor schemes, yielding more physically plausible spatial transitions. This advantage has been documented in performance comparisons where bicubic better preserves structure than bilinear methods (e.g., Xia et al., 2013) and is consistent with cautions on downscaling from coarse GCM fields (Salathé, 2003; Schoof, 2015; Schoof & Robeson, 2016).

3.2. Rainfall Distribution Identification

Distribution identification is carried out for $x_{o,k}$, $x_{m,k}$ and $x_{m,p}$ Datasets within defined time windows, following the QDM method. The time windows used include the validation and projection periods, which are divided by decade: the 2030s (2015–2030), the 2040s (2031–2040), and the 2050s (2041–2050). Probability distributions used are Extreme Value (EV), Generalized Extreme Value (GEV), Logistic (LOG), Normal (NOR), Exponential (EXP), Gamma (GAM), Inverse Gaussian (ING), Log-Logistic (LL), Lognormal (LN), and Weibull (WB). The best-fitting distribution is selected based on the one-sample Kolmogorov-Smirnov (K-S) test.

Monthly rainfall distributions are typically asymmetric and right-skewed, with most values clustered around 100–300 mm and relatively few very low or very high events in Lake Toba studies (Irwandi et al., 2023; Rafhida et al., 2024). Accordingly, we selected a set of ten distributions that capture diverse tail behaviors and shapes for non-negative data: the Gamma, Lognormal, Weibull, GEV (including Gumbel as Type-I extremes), Log-logistic, Inverse Gaussian, and several similar alternatives. For comparison, we also include a symmetric, bell-shaped distribution (e.g., the Normal distribution) to assess the consequences of imposing symmetry on inherently skewed data. This selection provides broad coverage of key characteristics (skewness, kurtosis/heavy tails, and support on $x \geq 0$), enabling goodness-of-fit tests and validation metrics to identify the most realistic model for the empirical rainfall distribution over Lake Toba.

This study employs two approaches for distribution identification: the full-period and the monthly approach. Previous studies on bias correction applied either the monthly separation method (Irwandi et al., 2023; Najib and Nurdiati, 2021; Nurdiati et al., 2019) or a full-period method without monthly separation (Cannon et al., 2015; Gumus et al., 2023). Both approaches are applied in this Lake Toba study, and findings show that their effectiveness varies depending on the location of the weather station (Rafhida et al., 2024). The monthly method was more effective at Doloksanggul station, while the full-period method was better suited to Silaen and Laguboti stations. Our approach does not explicitly model zero inflation. At the same time, this is reasonable for monthly data in an equatorial setting with few zero months; for daily-scale or strongly seasonal/arid applications, a two-part (occurrence-intensity) framework should be adopted.

As illustrated in Fig. 3, two distribution identification strategies are applied in rainfall bias correction. Type 1 (Monthly) separates the data into 12 distinct time segments based on month, producing a unique distribution for each month. This method, used in studies such as Najib and Nurdiati (2021) and Nurdiati et al. (2019), has been widely applied for sea surface temperature correction. On the other hand, Type 2 (Full-period) does not separate by month and uses a single distribution to represent the entire dataset. This approach was adopted by Cannon et al. (2015) and Gumus et al. (2023) to correct extreme climate variables.

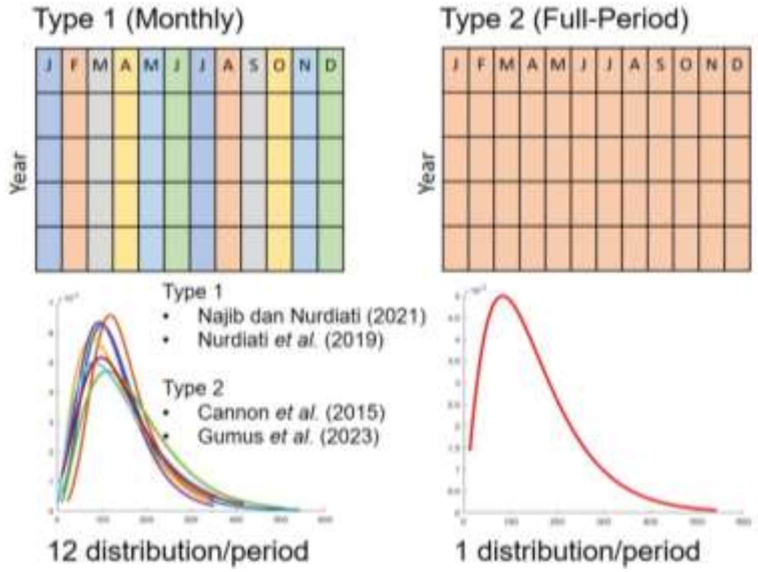

Figure 3. Two methods of distribution identification

3.3. Bias Correction

Statistical bias correction is carried out by establishing a relationship between observed and simulated rainfall data to derive a correction factor, y = f(x). This function links the cumulative distribution functions (CDFs), denoted as F, from both observational and model data. The CDF is calculated by integrating the corresponding probability distribution function:

$$F(x) = P(X \leq x) = \int_0^x f(t)dx\,,\ 0 < x < \infty$$

where x is the non-negative monthly rainfall. In this study, rainfall bias correction is applied to improve the predictive model. Bias correction plays a crucial role in minimizing systematic differences between climate model outputs and observations, thus improving the accuracy of future projections. The Quantile Delta Mapping (QDM) method is adopted in this research for bias correction.

3.3.1. Quantile Delta Mapping (QDM)

Quantile Delta Mapping (QDM) was first introduced by Li et al. (2010). Compared with other Quantile Mapping (QM) methods, Cannon (2018) demonstrated that QDM better preserves trends in climate model outputs. The QDM formulation, as outlined by Cannon et al. (2015), is given by:

$$\begin{gathered}\tau_{m,p}(t) = F_{m,p}^{(t)}\left(x_{m,p}(t)\right)\\ \hat{x}_{o:m,k:p}(t) = F_{o,k}^{-1}\left(\tau_{m,p}(t)\right)\\ \Delta_m(t) = \frac{x_{m,p}(t)}{F_{m,k}^{-1}\left(\tau_{m,p}(t)\right)} \qquad (1)\\ \hat{x}_{QDM_{m,p}}(t) = \hat{x}_{o:m,h:p}(t) * \Delta_m(t)\end{gathered}$$

where, $x_{m,p}(t)$ and $\hat{x}_{QDM_{m,p}}(t)$ represent the model-predicted rainfall before and after bias correction at time t, respectively. $\hat{x}_{o:m,k:p}(t)$ is the bias-corrected value from the historical observation, and $\Delta_m(t)$ denotes the relative change in model output between the historical and projection periods. The CDFs used in QDM include $F_{m,k}$, $F_{o,k}$, and $F_{m,p}^{(t)}$, representing the model calibration period, observation calibration period, and model projection at time window t, respectively.

4. Results

4.1. Coarse Resolution of CMIP6 data in Lake Toba region

CMIP6 models generally have a spatial resolution of about 1–2° (approximately 100–200 km), which is insufficient to capture the detailed climatic characteristics in regions with complex topography, such as North Sumatra. This coarse resolution fails to adequately represent rainfall variability driven by local factors such as mountains, valleys, and significant rain shadow effects surrounding Lake Toba (Wild and Hall, 1982). When coarse-resolution models are used to predict rainfall in areas such as Lake Toba, the results often exhibit large biases, particularly in estimating daily rainfall intensity and seasonal rainfall variability. These inaccuracies may affect analyses of climate trends, future climate change simulations, and hydrometeorological impact projections, such as flood or drought projections.

A significant challenge in using global climate models is that precipitation is provided as cell-mean values over very coarse grid cells. In our domain, the CMIP6 grid cells are large enough to cover most, if not all, of the Lake Toba basin, so they tend to represent the lake area as a single broad average rather than the fine-scale variability around the shoreline and in complex topography. This scale mismatch raises a high risk of bias (e.g., smoothed extremes and muted orographic contrasts). It indicates that the simulated rainfall may not accurately capture local rainfall variability around the lake. As illustrated in Fig. 4, the model grid boxes (colored by model) overlay much of the basin, explaining why cell-mean rainfall can misrepresent local conditions at BMKG stations.

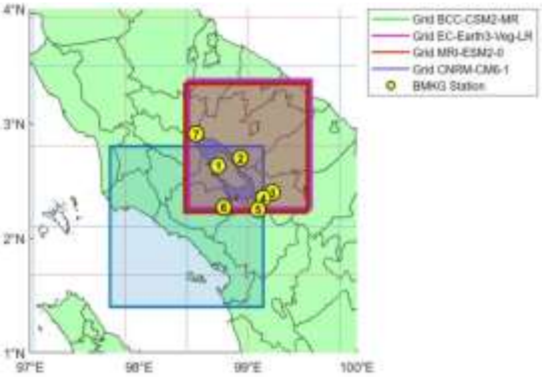

Figure 4. Overlay of CMIP6 model grid boxes over the Lake Toba region. Each colored box denotes the areal extent of a different model's grid cell, shown together with the lake/basin boundary (purple) and BMKG station locations (yellow, numbered 1–7 as in Fig. 1). The coarse cell sizes (∼1–2°) cover much of the basin, indicating a higher risk of bias and that simulated rainfall may not accurately capture local rainfall variability around the lake

This resolution limitation also affects rainfall estimation accuracy, especially in capturing spatial and temporal variations critical for climate and hydrometeorological analyses. Since these models have no data points within Lake Toba, their rainfall estimates may reflect climate characteristics of lower-elevation or different regions, leading to potential underestimation or overestimation of rainfall projections. This could influence the interpretation of research findings and climate-based planning in the region.

Therefore, CMIP6 data were interpolated at specific observation station locations to obtain more representative rainfall estimates before applying bias correction. The interpolation aims to adjust the coarse-resolution model grid values to the more specific observation points. This study employed the bicubic spline interpolation method, which provides smoother value transitions than linear or bilinear methods (Xia et al., 2013).

4.2. Data Overview Before Correction

After data extraction and interpolation, the interpolated CMIP6 model data can be directly compared with BMKG observational data. The results are shown in Fig. 5, which compares monthly rainfall between the observational data and several CMIP6 climate models: BCC-CSM2-MR, CNRM-CM6-1, EC-Earth3-Veg-LR, and MRI-ESM2-0. Boxplots indicate that the BCC-CSM2-MR model overestimates rainfall in April, May, and November, with higher medians and upper quartiles than observed. Furthermore, numerous upper outliers in April and May suggest the model simulates more frequent extreme rainfall events than observed.

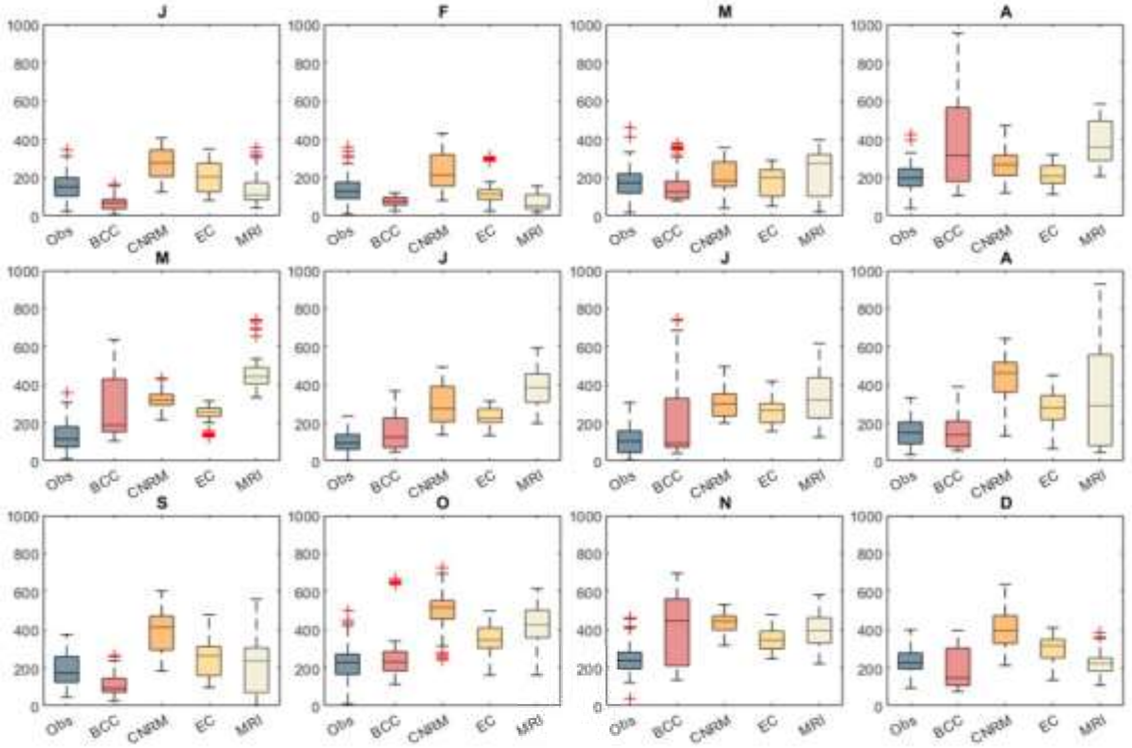

Figure 5. Boxplots showing distributions of rainfall data between BMKG observations and CMIP6 model outputs in the Lake Toba region

Additionally, months like April, November, and December exhibit significant rainfall variances, especially in the BCC-CSM2-MR and MRI-ESM2-0 models, which show broad rainfall distributions. The high variance in April and November is likely due to how the models interpret the wet-to-dry season transitions in Indonesia, where annual rainfall variability is typically higher. These models also seem less stable in capturing rainfall patterns during transition periods, resulting in broader distributions than those observed.

Conversely, there are months where the models underestimate rainfall, such as January, February, July, and September. During these months, BCC-CSM2-MR and EC-Earth3-Veg-LR show lower medians than the observed data. These underestimations likely result from the models' limitations in capturing local influences such as topography and monsoonal wind patterns that drive rainfall formation. Additionally, the coarse spatial resolution of the models may lead to inaccuracies in representing small-scale convective systems, especially during the dry season transition. To assess baseline accuracy before bias correction, Table 2 summarizes the monthly MAE between uncorrected (spatially interpolated) CMIP6 precipitation and observations over the Lake Toba region.

Table 2. Monthly mean absolute error (MAE) of uncorrected CMIP6 precipitation (after spatial interpolation to the study domain) relative to observations

Month	**Mean Absolute Error**			
	BCC-CSM2-MR	EC-Earth3-Veg-LR	CNRM-CM6-1	MRI-ESM2-0
January	99.92	134.15	87.39	85.97
February	81.61	127.56	81.96	94.06
March	112.76	109.80	91.22	129.69
April	240.26	101.15	70.96	172.63
May	184.90	202.78	136.88	331.11
June	94.40	197.42	133.24	285.14
July	157.45	198.01	152.83	242.60
August	65.77	279.23	129.38	263.02
September	108.82	210.91	125.73	130.30
October	125.99	276.85	147.70	213.99
November	188.24	195.28	130.70	164.86
December	111.65	181.48	99.88	76.73
Full-Period	99.92	134.15	87.39	85.97

MAE varies markedly across seasons and models, as shown in Table 2. The most significant errors occur in transition months and early-mid dry season: MRI-ESM2-0 spikes in May-August and October (≈165–331 mm), EC-Earth3-Veg-LR also peaks in August-October (≈277–279 mm), while BCC-CSM2-MR is notably high in April (≈240 mm). By contrast, CNRM-CM6-1 tends to track observations more closely in many months (often <150 mm, down to ~71 mm in April). These patterns indicate substantial wet biases for specific models and months, underscoring the need for bias correction before interpreting rainfall projections.

Overall, this analysis shows that the models exhibit various biases in representing rainfall, including overestimation, underestimation, and high variance. The BCC-CSM2-MR model generally produces higher values than observations during months with high variability, whereas EC-Earth3-Veg-LR often underestimates rainfall at the beginning and end of the year (December, January, February (DJF)). To further diagnose these biases in a seasonal context, we present the monthly annual cycles for each model alongside observations in Fig. 6.

Figure 6 shows the model-specific annual cycles (colored lines with ±1σ bands) compared to the observed cycle (black). MRI-ESM2-0 peaks well above observations in September-October, indicating difficulty in reproducing the observed bimodal pattern late in the year. EC-Earth3-Veg-LR underestimates through early-mid year and partially recovers toward SON, consistent with the boxplot patterns. BCC-CSM2-MR tends to overshoot during wet-season months (e.g., MAM and parts of SON), with broader uncertainty bands that suggest inflated variability. CNRM-CM6-1 shows a more monotonic rise from JJA to DJF than observed, missing the secondary peak structure. Together, these cycles confirm that pre-correction model outputs smooth or misplace the bimodal rainfall peaks over Lake Toba, motivating the subsequent bias-correction step.

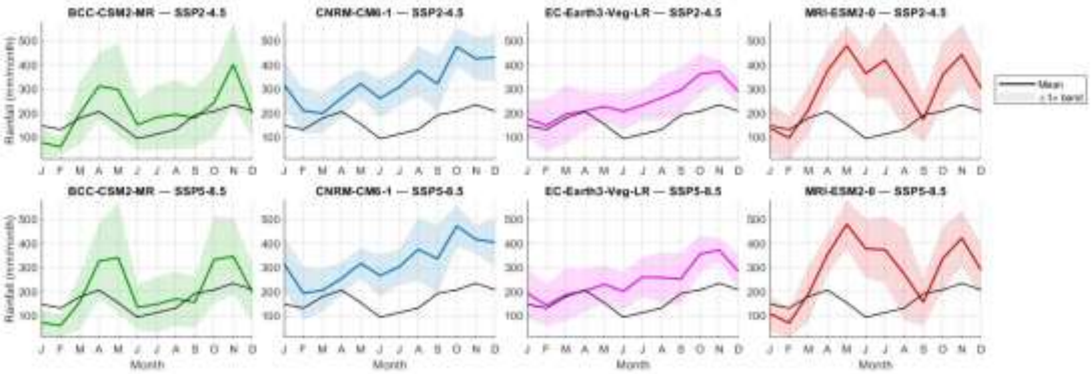

Figure 6. Monthly climatology (annual cycle) of rainfall over Lake Toba for each CMIP6 model (colored line; shaded band = ±1σ across years) compared with observations from Fig. 2 (black line; seven-station arithmetic mean). Top row: SSP2-4.5; bottom row: SSP5-8.5

4.3. Identification of Distribution Algorithm

The next step is identifying the monthly rainfall distribution using various probability distributions. For this example, the rainfall data used are for January during the calibration period (1973–2003) (see Fig. 7). The distribution used is described in the methods chapter. The distribution identification process follows the algorithm below:

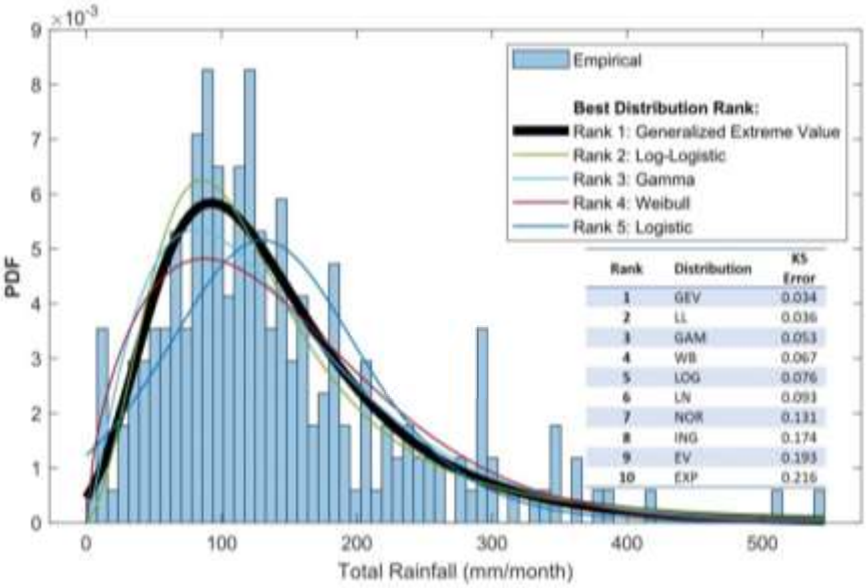

Rank	Distribution	KS Error
1	GEV	0.034
2	LL	0.036
3	GAM	0.053
4	WB	0.067
5	LOG	0.076
6	LN	0.093
7	NOR	0.131
8	ING	0.174
9	EV	0.193
10	EXP	0.216

Figure 7. Histogram of monthly rainfall data for the calibration period (1973–2003) in January, plot of five distributions with the smallest KS error, and the rank of KS error of ten distributions

Distribution Identification Algorithm:

(i) Estimate the parameters of ten candidate distributions using the Maximum Likelihood Estimator (MLE).

(ii) Calculate the goodness-of-fit using the one-sample Kolmogorov-Smirnov (K-S) test, which computes the maximum error between the empirical and theoretical distributions.

(iii) Rank the distributions based on their K-S test values.

(iv) Select the distribution with the smallest K-S error as the best fit.

Fig. 6 compares the empirical distribution (blue histogram) with several theoretical distributions fitted to the monthly rainfall data. Based on the K-S error results, the Generalized Extreme Value (GEV) distribution has the smallest K-S error (0.034), indicating the best fit for January rainfall data. Other distributions, such as Log-Logistic, Gamma, Weibull, and Logistic, also show reasonably good fits, but with slightly larger deviations than GEV. In this case, the GEV distribution is selected as the best-fitting distribution. This process is repeated for $x_{o,k}$, $x_{m,k}$, and $x_{m,p}$ for the validation time windows, namely the 2030s, 2040s, and 2050s.

Table 3 presents the monthly and full-period rainfall distribution identification results for the Lake Toba region, both for observational and model data. The results indicate that the monthly rainfall distribution in the observational data is well described by the Generalized Extreme Value (GEV) distribution, which aligns with the characteristics of extreme rainfall and long right tails observed in the study area. GEV appears consistently throughout the year, except in October and November, where the Logistic (LOG) distribution is observed. This suggests that the empirical rainfall distribution in the region tends to capture asymmetric extreme characteristics.

Table 3. Identification of the data distribution of observation and model rainfall data

Month	**Distribution**				
	Observation	BCC-CSM2-MR	EC-Earth3-Veg-LR	CNRM-CM6-1	MRI-ESM2-0
January	GEV	LN	LL	NOR	ING
February	GEV	LL	LL	GEV	LN
March	WB	GAM	WB	EV	GEV
April	GEV	NOR	WB	EV	WB
May	GEV	GAM	EV	LOG	LOG
June	GEV	GEV	LOG	GEV	GAM
July	GEV	GEV	LOG	GEV	LL
August	GEV	LL	NOR	LL	GEV
September	GEV	GEV	LOG	EV	GEV
October	LOG	GAM	GEV	GEV	LL
November	LOG	ING	GAM	GEV	GEV
December	GEV	LL	GEV	GEV	LN
Full-Period	GEV	LN	WB	LOG	NOR

Meanwhile, the BCC-CSM2-MR model predominantly exhibits Lognormal (LN) and Log-Logistic (LL) distributions, with occasional GEV occurrences. Other models show considerable variability in their monthly distributions. For example, EC-Earth3-Veg-LR tends to use Weibull (WB) and Extreme Value (EV) distributions. The CNRM-CM6-1 model displays a highly varied distribution pattern, combining NOR (Normal), EV, LOG, and GEV, suggesting instability in capturing monthly rainfall distributions. MRI-ESM2-0 shows a relatively consistent presence of GEV in the second half of the year, but still exhibits variation with the presence of LN, LL, and LOG in other months.

4.4. Bias Correction Process

The QDM calculation begins with the identification of the time-dependent cumulative distribution function (CDF) $F_{m,p}^{(t)}$ of the model data $x_{m,p}$, where p refers to the prediction period. In this study, the period p is categorized into four sub-periods: a validation period (2004–2014) to evaluate model performance, and three future projection periods 2030s (2015–2030), 2040s (2031–2040), and 2050s (2041–2050).

For instance, to correct the CMIP6 validation data in January 2006 or $t_{1,2006}$, we have $x_{m,v}(t_{1,2006}) = x_{m,v}(t_{1,2006}) = 138.07$. Distribution $F_{m,v}^{(t)}$ is identified and determined to follow a Logistic (LOG) distribution with parameters $= 68.09$ and $s = 22.75$. This distribution is used to calculate the quantile. $\tau_{m,v}(t)$ as follows:

$$\tau_{m,v}\left(t_{1,2006}\right) = F_{m,v}^{(t)}\left(x_{m,v}\left(t_{1,2006}\right)\right) = F_{m,v}^{(t)}(138.07) = 0.96 \qquad (2)$$

Subsequently, the distribution $F_{m,k}$ is assumed to follow a Lognormal (LN) distribution with parameters $\mu = 4.27$, and $\sigma = 0.65$. As we have quantile value $\tau_{m,v}$ in Eq.2, the relative change in quantile between the calibration period and time t in January 2006 is calculated as:

$$\Delta_m\left(t_{1,2006}\right) = \frac{x_{m,v}\left(t_{1,2006}\right)}{F_{m,k}^{-1}\left(\tau_{m,v}\left(t_{1,2006}\right)\right)} = \frac{138.07}{F_{m,k}^{-1}(0.96)} = \frac{138.07}{217.96} = 0.63 \qquad (3)$$

The theoretical CDF of the observed rainfall data during the calibration period, $\left(F_{o,k}\right)$, follows a Generalized Extreme Value (GEV) distribution with parameters $\xi = 0.009$, $\sigma = 63.29, \mu = 98.35$. The quantile value $\tau_{m,v}$ can then be bias-corrected using:

$$\widehat{x}_{o:m,k:v}\left(t_{1,2006}\right) = F_{o,k}^{-1}\left(\tau_{m,v}\left(t_{1,2006}\right)\right) = F_{o,k}^{-1}(0.96) = 327.93 \qquad (4)$$

The final QDM-corrected rainfall value for January 2006 is obtained by multiplying the relative change Δ_m by the bias-corrected quantile $\hat{x}_{o:m,k:v}$:

$$\hat{x}_{QDM_{m,v}}\left(t_{1,2006}\right) = \Delta_m \times \hat{x}_{o:m,k:v} = 0.63 \times 327.93 = 206.6 \qquad (5)$$

For comparison, the basic quantile mapping (QM) method utilizes only the calibration distributions of historical observations $F_{o,k}$ and the model $F_{m,k}^{-1}$. Using the same distributions, the QM-corrected rainfall is computed as:

$$\hat{x}_{QM_{m,v}}\left(t_{1,2006}\right) = F_{o,k}^{-1}\left(F_{m,k}^{-1}\left(x_{m,v}\left(t_{1,2006}\right)\right)\right) = F_{o,k}^{-1}\left(F_{m,k}(138.07)\right) = F_{o,k}^{-1}(0.84) = 220.22 \qquad (6)$$

The key difference between QM and QDM lies in the calculation of Δ_m, which represents the relative change between the projected and calibrated distributions. This enables QDM to account for temporal shifts in rainfall distribution. Consequently, QDM can better capture complex climate dynamics, such as distributional shifts in extreme events or long-term rainfall trends. In contrast, QM merely maps quantiles from the model to the observations without accounting for distributional evolution over time, which may introduce bias in long-term climate projections.

4.5. Comparison Between Monthly and Full-Period Correction

In this section, we compare the results of the two correction approaches with the uncorrected model data. A seasonal comparison between observed rainfall and CMIP6 model outputs is illustrated in Fig. 8. The analysis is performed seasonally, as the rainfall pattern in Fig. 2 reflects the equatorial climate, which typically features two rainy season peaks (March-April-May (MAM), September-October-November (SON)) and two dry season valleys (December-January-February (DJF), and June-July-August (JJA)).

As shown in Fig. 8, before bias correction (Pre), the CMIP6 models exhibit significant deviations from the observed data. These deviations are visible in the differences in median, interquartile range, and the number of outliers, particularly in the CNRM-CM6-1 model (highlighted in orange), which consistently overestimates rainfall across all seasons (DJF, MAM, JJA, and SON).

Moreover, the uncorrected model data show wider distributions than the observations, indicating bias in how the models represent rainfall in the Lake Toba region. After applying the QDM method with both monthly (QDM1) and full-period (QDM2) distribution identification, the model data distribution improves significantly. The corrected models show medians and interquartile ranges that align more closely with the observations, along with fewer outliers. This demonstrates the method's effectiveness in reducing systematic bias in CMIP6 outputs. Notably, QDM1 captures early-year rainfall more accurately than QDM2, which tends to underestimate. Conversely, QDM2 tends to overestimate late-year rainfall. Overall, the monthly approach (QDM1) provides greater consistency with observed distributions.

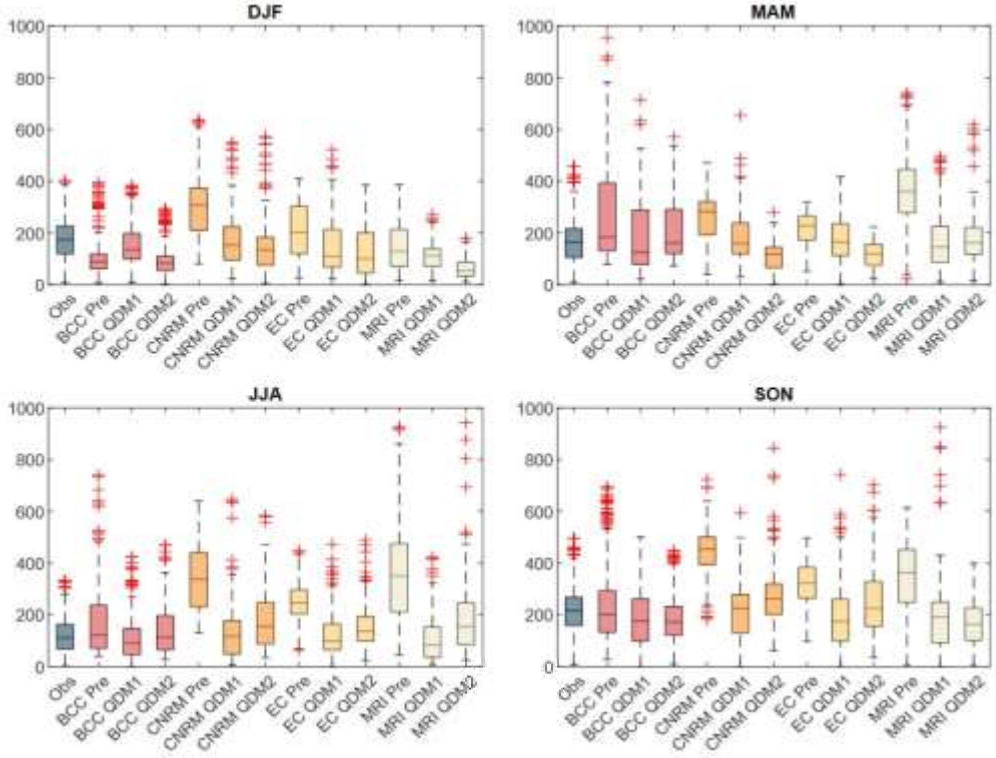

Figure 8. Boxplot of observed and model data by season during the validation period (2004–2014). The "Pre" boxplot represents data before correction, while "QDM1" and "QDM2" represent bias correction using monthly and full-period distribution identification, respectively

To assess the effectiveness of the bias correction, we applied two evaluation metrics: the Mean Absolute Error (MAE) and the two-sample Kolmogorov-Smirnov (KS) test. MAE measures the average error between the model and observed data, with larger MAE values indicating greater bias. The KS test evaluates the maximum difference between the empirical distributions of the model and observation data, with values ranging from 0 to 1 higher values indicate greater distributional discrepancy. In this study, the difference in MAE before and after correction was used to evaluate correction effectiveness, with positive differences indicating improvement (i.e., reduced MAE). The MAE differences are visualized in Fig. 9a, and the KS test results are shown in Fig. 9b.

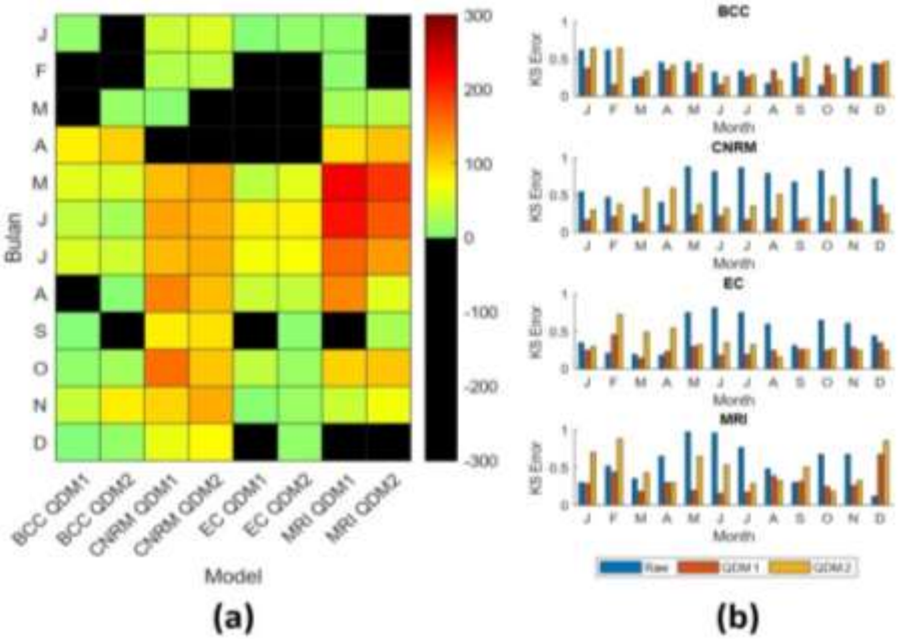

Figure 9. Evaluation of two different methods of distribution identification monthly (QDM1) and full-period (QDM2): (a) heatmap of MAE difference magnitude, and (b) barplot of two-sample Kolmogorov-Smirnov test results

Figure. 9a presents a heatmap of the MAE difference between model data and observations for each month and model. Red cells indicate successful correction (lower MAE), green indicates minimal change, and black signifies increased error after correction. Overall, both monthly (QDM1) and full-period (QDM2) correction methods reduce MAE across most models and months. QDM1 is more effective for the CNRM-CM6-1 and MRI-ESM2-0 models, mainly from May to September, while QDM2 performs better with the BCC-CSM2-MR model. However, both methods are less effective at the start and end of the year, coinciding with peak rainfall periods. This is supported by a recurrent band of black cells in January-April, and again in August-September and December, across several models.

These pockets of deterioration likely arise from: (i) seasonal-regime shifts during DJF and the MAM/SON transition months, when month-to-month quantile structure changes rapidly; monthly fits can become less stable and full-period fits can be too smoothed, either of which can increase MAE; (ii) representativeness and orographic effects that are strongest during convective peaks and transition seasons (Le et al., 2025), so anchoring corrections to biased tails can amplify mismatch at stations. Model-specific behavior is evident too: for example, CNRM and MRI show more frequent black cells early in the year, in line with their raw KS patterns (Fig. 9b). Taken together, the heatmap shows that while net improvements dominate, certain seasons and models remain challenging, motivating the use of both identification strategies and the cautious interpretation of corrected outputs in DJF and transition months.

Figure 9b shows the results of the two-sample Kolmogorov-Smirnov (KS) test before and after correction in all station data. For the KS evaluation, we pooled monthly rainfall data from all seven BMKG stations into a single dataset before computing the KS error. This approach ensures a robust assessment of distributional differences across the entire study region. Before correction (Raw), KS errors were high, particularly in January, February, May-November, and December, indicating significant distributional bias. Both QDM1 and QDM2 substantially reduced KS errors for almost all models, with QDM1 showing more consistent performance. We calculated the average improvement in KS error for each model by comparing pre- and post-correction values. The reduction was expressed as a percentage of the pre-correction value and averaged across all 12 months. Finally, we average across all models to obtain the overall figure. Using this procedure, the average KS error reduction is 47.26% for QDM1 and 20.39% for QDM2. However, certain months, such as March and April for the BCC-CSM2-MR model and February and April for EC-Earth3-Veg-LR, still showed high KS errors even after correction. Using a paired Wilcoxon signed-rank test on the KS distances, the monthly-based correction (QDM1) performs significantly better than the full-period approach (QDM2) across all pairs examined ($p = 4.92\times10^{-6}$).

The post-correction increase in distributional mismatch for CNRM (March-April), EC-Earth (February-April), and MRI (January, February, December) (Fig. 9b) likely has several causes. First, pronounced seasonal shifts create shape mismatches between observed and modeled distributions; in such transition months, quantile mapping becomes highly non-linear, and the QDM delta factor can over-adjust specific quantiles when the calibration and application distributions differ (Cannon et al., 2015). Second, zero inflation and extreme tails dominate during wet months, reducing KS sensitivity around the center but increasing deviations at the tails so KS errors can remain high even after correction (Rafhida et al., 2024). Third, spatial representativeness errors from mapping GCM grid cells to station locations over complex terrain can leave residual structural bias (notably for CNRM) that quantile-based correction cannot entirely remove. These findings argue for additional safeguards in transition months (e.g., sensitivity tests for distributional choices, explicit dry-day handling, tail capping, or seasonal/rolling-window calibration) to avoid worsening the distributional fit.

Overall, QDM effectively improves the rainfall distribution in CMIP6 models, making them more closely resemble observed data. However, the direction of bias whether underestimation or overestimation requires further evaluation using relative quantile change analysis as proposed by Cannon et al. (2015). The relative change is calculated as the ratio of historical to future quantiles. For model data, this ratio is derived from the validation versus calibration periods; for corrected data, it is calculated from the ratio of corrected data to observed quantiles. If the relative change after correction is larger than that of the original model data, it indicates an overestimation. Conversely, a minor relative change implies underestimation.

As shown in Fig. 10, the relative changes between raw CMIP6 data and bias-corrected data are compared across three quantiles: low rainfall at $\tau = 0.25$ (Fig. 10a), moderate-to-high rainfall at $\tau = 0.75$ (Fig. 10b), and extreme rainfall at $\tau = 0.99$ (Fig. 10c). Each dot in the plot represents the relative change for a specific month and model using QDM1 (blue) and QDM2 (red). The dashed diagonal line represents the reference line points on this line indicate that the relative change is preserved after correction.

At the quantile 0.25 (Fig. 10a), most points lie below the diagonal line, indicating that bias correction generally yields lower values than the original model's relative changes, suggesting underestimation at low rainfall levels. QDM2 shows more deviation from the diagonal than QDM1, indicating that QDM2 is more prone to overestimating low rainfall during mid-year months. At quantile 0.75 (Fig. 10b), both methods show stable relative changes, though QDM2 again shows greater deviations. QDM1 is more consistent in preserving the original quantile structure. At quantile 0.99 (Fig. 10c), most points lie above the diagonal, indicating that both methods tend to overestimate extreme rainfall. However, the deviation varies more than at the lower quantile, with some cases of underestimation. QDM1 tends to overestimate high rainfall, but with less deviation than QDM2. In conclusion, the monthly distribution identification method (QDM1) performs better for rainfall correction in the Lake Toba region.

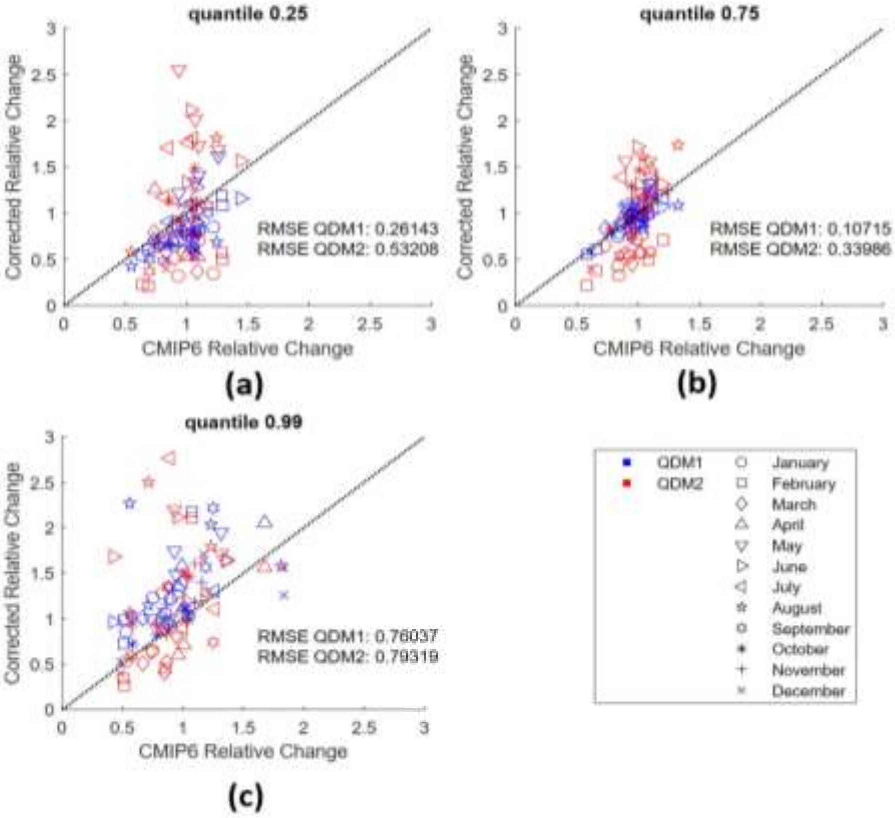

Figure 10. Relative change (Δ) between CMIP6 data and after correction data at two extreme quantiles, (a) $\tau = 0.25$, (b) $\tau = 0.75$, and (c) $\tau = 0.99$. If the bias correction results maintain relative changes, the point should be on the line. If it is above then it is overestimated, and if otherwise then it is underestimated

These patterns are consistent with the RMSE summaries in each panel, computed as RMSE relative to the 1:1 line. At τ = 0.25, RMSE(QDM1) = 0.261 and RMSE(QDM2) = 0.532, showing QDM1 cuts the average deviation from the diagonal by roughly half, i.e., it better preserves low-quantile change signals. At τ = 0.75, errors drop further and the gap widens: RMSE(QDM1) = 0.107 versus RMSE(QDM2) = 0.340, highlighting

QDM1's stronger fidelity for mid-quantile changes. At τ=0.99, both methods struggle, as expected, at the extremes, but QDM1 still performs slightly better (0.760 vs 0.793). Taken together, the consistently lower RMSE for QDM1 across all quantiles confirms that monthly identification yields changes closer to the model-implied signal, with the most significant benefit at the mid-quantile and a modest advantage even at the extreme tail.

From an applied perspective, these tendencies matter. Underestimation at low rainfall (τ = 0.25) can bias drought metrics, dry-season water-supply assessments, irrigation scheduling, and crop-model stress indices toward overly optimistic conditions. Overestimation at the high end (τ = 0.99) can inflate design floods, trigger false positives in early-warning thresholds, or overstate sediment/runoff hazards. To mitigate decision risk when using the corrected data, we (i) recommend prioritizing QDM1 outputs, (ii) propagating the residual uncertainty by reporting and using the ±1σ (or quantile) spread and the residual MAE/KS when driving hydrologic/agronomic models, and (iii) exercising extra caution for DJF and transition months where deviations are most pronounced.

4.6. Future CMIP6 projection

After applying bias correction, the four models used in this study were combined using the Multi-Model Ensemble (MME) method. MME is a widely used technique in climate modeling to reduce uncertainty by integrating outputs from multiple models (Tebaldi and Knutti, 2007). This study specifically employed the Multi-Model Ensemble Mean (MMEM). The MMEM projection results were then compared to the baseline data, which refers to observed data from the calibration period (1973–2003) (Fig. 11).

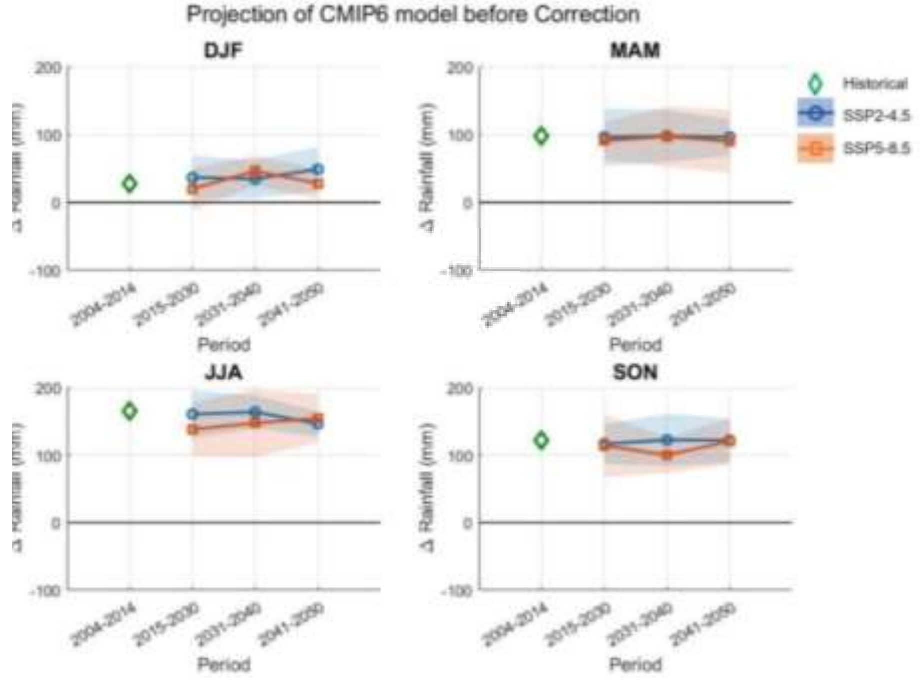

Figure 11. Relative changes in CMIP6 model projection rainfall before correction with observation data for the calibration period (1973–2003) as baseline data. The top and bottom boundaries of the shaded area are the ± standard deviation of the GCMs

As shown in Fig. 11, the Multi-Model Ensemble Mean (MMEM) changes in projected rainfall based on CMIP6 models are presented for the four main seasons (DJF, MAM, JJA, SON) under two emission scenarios (SSP2-4.5 and SSP5-8.5) for the near future period (2015–2040), compared to the baseline observational data (1973–2003). The shaded ribbons show the inter-model spread (±1 standard deviation) around the MMEM for each SSP. Overall, the models show a tendency to increase, especially in DJF and SON seasons. In DJF, rainfall sharply increases under SSP5-8.5 during 2015–2030, but then declines in 2031–2040. In contrast, SSP2-4.5 shows a more stable increase. Rainfall in MAM remains relatively stable, while JJA consistently shows a decrease across both scenarios. SON exhibits fluctuations, with SSP2-4.5 showing an increasing trend, while SSP5-8.5 experiences a slight decline. Generally, the projections suggest a potential increase in future rainfall in the Lake Toba region.

Figure 12 displays the projections after bias correction using the QDM1 method, which significantly improved the alignment between model projections and observed data. The correction effectively reduced overestimation during the DJF and MAM seasons and yielded projections closer to the baseline data. For instance, in DJF during the 2031–2040 period, SSP2-4.5 showed a slight increase in rainfall (+2.82 mm), whereas SSP5-8.5 actually showed a decrease (-17.28 mm) compared to the baseline. For JJA, the correction resulted in more varied trends, with rainfall increasing in some periods and decreasing in others. Overall, comparisons with the baseline are used solely to quantify the projected rainfall changes attributable to greenhouse gas forcing.

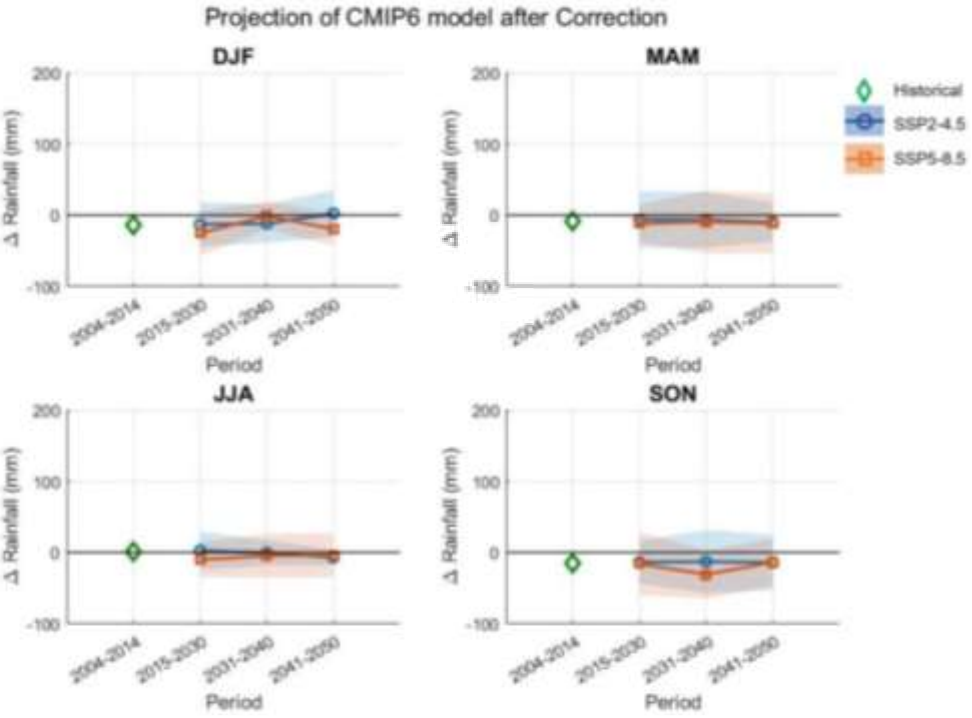

Figure 12. Same as (Fig. 11) but with corrected data

5. Discussions

Regional assessments using uncorrected CMIP6 generally point to wetter futures around Sumatra/Lake Toba (e.g., Ona et al., (2024) who show broad SEA wetting with only seasonal drying patches over Sumatra, especially in MAM by around -4%, besides increasing in other season; Mareta et al., (2024), pan-Sumatra increases by around 20–40 mm). In contrast, after bias correction, our study yields a more conservative signal: future rainfall for Lake Toba is expected to decrease slightly. Similar results were presented by Gumus et al. (2024), who found that in a study conducted in Turkey, bias-corrected CMIP6 data produced lower rainfall projections than the raw data under both emission scenarios. It is consistent with evidence that QM/QDM tends to damp wet biases and reduce projected totals in the equatorial belt. For example, (2017) showed that quantile-mapping across Southeast Asia systematically shifts precipitation distributions toward drier conditions and reduces wet-season peaks. A recent Sumatra-focused CMIP6 study applying LS/QDM likewise reports moderated (often lower) post-correction rainfall compared with raw outputs (Hidayat and Taufik, 2025). Together, these results suggest that without correction, CMIP6 can overstate wetting around Lake Toba, whereas QDM-corrected projections better reflect local hydroclimate constraints and point to modest declines, especially in MAM.

In response to concerns that "correcting rainfall by altering the climate model's change signal" might produce an apparent rainfall decrease "without a physical mechanism," we emphasize that bias correction particularly the Quantile Delta Mapping (QDM) method does not remove the large-scale dynamics simulated by GCMs. Instead, it adjusts the distribution's amplitude and shape to be consistent with local observational statistics (Cannon, 2018; Cannon et al., 2015; Teutschbein and Seibert, 2012).

In the context of Lake Toba, which is mountainous and situated behind the Barisan Range thus strongly influenced by the rain-shadow effect the monthly distribution-based QDM (as applied in our study) preserves the relative per-quantile changes from the GCM. However, when anchored to the local observational distribution and aggregated seasonally, the results may weaken the GCM's wetting signal and, during MAM, shift toward a "slight decrease." This reflects local hydroclimatic constraints (orography/rain shadow) rather than the absence of a physical mechanism. Therefore, the sign difference between the raw projections (slightly increasing) and the bias-corrected results (moderate to slightly decreasing) aligns with QDM theory (quantile-wise signal preservation) and the supporting literature cited above, as well as our interpretation that the monthly QDM more effectively represents Lake Toba's rainfall characteristics than the full-period approach.

Overall, bias correction using the QDM method with a monthly distribution approach yields more accurate results for the Lake Toba region than the full-period approach. These findings underscore the importance of selecting bias-correction methods that align with local climate characteristics and of integrating high-quality observational data from weather stations for validation. Moving forward, it is recommended that this approach be complemented by regional climate models (RCMs) or machine learning-based methods to capture complex distribution patterns better, and that the projection scope be extended to the end of the 21st century by incorporating additional climate variables such as temperature, humidity, and global indices like ENSO and IOD.

6. Conclusions

This study shows that the Generalized Extreme Value (GEV) distribution best represents the extreme rainfall characteristics for most months in the Lake Toba region. At the same time, the logistic and Weibull distributions are also relevant for certain months. Monthly-based distribution identification outperformed the full-period approach in capturing the rainfall characteristics. The Quantile Delta Mapping (QDM) bias correction method, applied via two approaches, monthly distribution fitting (QDM1) and full-period distribution fitting (QDM2), successfully adjusted climate model distributions to more closely align with observations while preserving temporal quantile changes. Evaluation using Mean Absolute Error (MAE) difference and two-sample Kolmogorov-Smirnov (KS) tests indicated that QDM, particularly QDM1, improved the model-observation distribution agreement by 47.26%, compared to 20.39% for QDM2.

Rainfall projections for the near future period (2015–2050) revealed differing trends across seasons and emission scenarios. Uncorrected CMIP6 models tend to overestimate, especially in DJF and MAM. However, after applying bias correction, projections became more realistic and closer to historical values, with reduced seasonal extremes, though uncertainties remain, particularly under SSP5-8.5. In general, bias correction enhances the reliability of climate projections for the Lake Toba region.

For future work, we recommend (i) dynamic downscaling with CORDEX-class regional climate models to better resolve Lake Toba's orography and lake-land contrasts, thereby sharpening extremes and spatial gradients that drive hydropower inflows; (ii) data-driven refinements to QDM e.g., nonparametric/ML quantile methods or hybrid occurrence-intensity models to handle distributional shifts and zero-inflation while preserving change signals and (iii) recommend extending to far-future (2071–2100) and incorporating temperature/humidity. Together, these steps should reduce model-to-model spread, improve sub-seasonal guidance for reservoir operations, and extend projections into the mid- to late century for planning horizons. Policy implication: Basin managers and utilities should adopt adaptive, climate-informed reservoir rule curves and flexible hydropower scheduling driven by ensemble sub-seasonal guidance and mid-century scenarios while prioritizing investments in data-sharing and regional downscaling to hedge drought and flood risks.

Acknowledgements

This research was funded by the Directorate of Research and Community Service, Directorate General of Research and Development, Ministry of Higher Education, Science, and Technology of the Republic of Indonesia, through contract number 23341/IT3.D10/PT.01.03/P/B/2025.

References

Ahn J.B., Jo S., Suh M.S., Cha D.H., Lee D.K., Hong S.Y., Min S.K., Park S.C., Kang H.S., Shim K.M., 2016. Changes of precipitation extremes over South Korea projected by the 5 RCMs under RCP scenarios. Asia-Pacific J. Atmos. Sci., 52, 223–236. https://doi.org/10.1007/s13143-016-0021-0.

Aldrian E., Susanto D.R., 2003. Identification of three dominant rainfall regions within Indonesia and their relationship to sea surface temperature. Int. J. Climatol., 23, 1435–1452. https://doi.org/10.1002/joc.950.

Cannon A.J., 2018. Multivariate quantile mapping bias correction: an N-dimensional probability density function transform for climate model simulations of multiple variables. Clim. Dyn., 50, 31–49. https://doi.org/10.1007/s00382-017-3580-6.

Cannon A.J., Sobie S.R., Murdock T.Q., 2015. Bias correction of GCM precipitation by quantile mapping: How well do methods preserve changes in quantiles and extremes? J. Clim., 28, 6938–6959. https://doi.org/10.1175/JCLI-D-14-00754.1

Chen J., Brissette F.P., Chaumont D., Braun M., 2013. Performance and uncertainty evaluation of empirical downscaling methods in quantifying the climate change impacts on hydrology over two North American river basins. J. Hydrol., 479, 200–214. https://doi.org/10.1016/j.jhydrol.2012.11.062.

Chesner C.A., 2012. The Toba Caldera Complex. Quat. Int., 258, 5–18. https://doi.org/10.1016/j.quaint.2011.09.025.

Döscher R., Acosta M., Alessandri A., Anthoni P., Arsouze T., Bergman T., Bernardello R., Boussetta S., Caron L.P., Carver G., Castrillo M., Catalano F., Cvijanovic I., Davini P., Dekker E., Doblas-Reyes F.J., Docquier D., Echevarria P., Fladrich U., Fuentes-Franco R., Gröger M., Hardenberg J.V., Hieronymus J., Karami M.P., Keskinen J.P., Koenigk T., Makkonen R., Massonnet F., Ménégoz M., Miller P.A., Moreno-Chamarro E., Nieradzik L., Van Noije T., Nolan P., O'donnell D., Ollinaho P., Van Den Oord G., Ortega P., Prims O.T., Ramos A., Reerink T., Rousset C., Ruprich-Robert Y., Le Sager P., Schmith T., Schrödner R., Serva F., Sicardi V., Sloth Madsen M., Smith B., Tian T., Tourigny E., Uotila P., Vancoppenolle M., Wang S., Wårlind D., Willén U., Wyser K., Yang S., Yepes-Arbós X., Zhang Q., 2022. The EC-Earth3 Earth system model for the Coupled Model Intercomparison Project 6. Geosci. Model Dev., 15, 2973–3020. https://doi.org/10.5194/gmd-15-2973-2022.

Eyring V., Bony S., Meehl G.A., Senior C.A., Stevens B., Stouffer R.J., Taylor K.E., 2016. Overview of the Coupled Model Intercomparison Project Phase 6 (CMIP6) experimental design and organization. Geosci. Model Dev., 9, 1937–1958. https://doi.org/10.5194/gmd-9-1937-2016.

Grose M.R., Narsey S., Delage F.P., Dowdy A.J., Bador M., Boschat G., Chung C., Kajtar J.B., Rauniyar S., Freund M.B., Lyu K., Rashid H., Zhang X., Wales S., Trenham C., Holbrook N.J., Cowan T., Alexander L., Arblaster J.M., Power S., 2020. Insights From CMIP6 for Australia's Future Climate. Earth's Futur., 8, e2019EF001469. https://doi.org/10.1029/2019EF001469.

Gumus B., Oruc S., Yucel I., Yilmaz M.T., 2023. Impacts of Climate Change on Extreme Climate Indices in Türkiye Driven by High-Resolution Downscaled CMIP6 Climate Models. Sustain, 15. https://doi.org/10.3390/su15097202.

Hermawan E., 2010. Pengelompokkan Pola Curah Hujan Yang Terjadi Di Beberapa Kawasan P. Sumatera Berbasis Hasil Analisis Teknik Spektral. J. Meteorol. dan Geofis, 11. https://doi.org/10.31172/jmg.v11i2.67.

Hidayat R., Taufik M., 2025. Bias Correction of CMIP6 Models for Assessment of Wet and Dry Conditions Over Sumatra. Agromet, 39, 33–39. https://doi.org/10.29244/j.agromet.39.1.33-39.

Ho C.K., Stephenson D.B., Collins M., Ferro C.A.T., Brown S.J., 2012. Calibration strategies a source of additional uncertainty in climate change projections. Bull. Am. Meteorol. Soc., 93, 21–26. https://doi.org/10.1175/2011BAMS3110.1.

Hofstra N., New M., McSweeney C., 2010. The influence of interpolation and station network density on the distributions and trends of climate variables in gridded daily data. Clim. Dyn., 35, 841–858. https://doi.org/10.1007/s00382-009-0698-1.

Irwandi H., Ariantono J.Y., Kartika Q.A., Siregar A.C.P., Tari C.A., Sudrajat A., 2017. Pengaruh Iklim Terhadap Penurunan Tinggi Muka Air Danau Toba, in: Seminar Nasional Sains Atmosfer, 105–110.

Irwandi H., Rosid M.S., Mart T., 2023. Effects of Climate change on temperature and precipitation in the Lake Toba region, Indonesia, based on ERA5-land data with quantile mapping bias correction. Sci. Rep., 13, 1–11. https://doi.org/10.1038/s41598-023-29592-y.

Karmalkar A.V., Thibeault J.M., Bryan A.M., Seth A., 2019. Identifying credible and diverse GCMs for regional climate change studies case study: Northeastern United States. Clim. Change, 154, 367–386. https://doi.org/10.1007/s10584-019-02411-y.

Le X.-H., Koyama N., Kikuchi K., Yamanouchi Y., Fukaya A., Yamada T., 2025. Evaluating Geostatistical and Statistical Merging Methods for Radar-Gauge Rainfall Integration: A Multi-Method Comparative Study. Remote Sens., 17. https://doi.org/10.3390/rs17152622.

Li H., Sheffield J., Wood E.F., 2010. Bias correction of monthly precipitation and temperature fields from Intergovernmental Panel on Climate Change AR4 models using equidistant quantile matching. J. Geophys. Res. Atmos., 115. https://doi.org/10.1029/2009JD012882.

Li X., Li Z., 2023. Evaluation of bias correction techniques for generating high-resolution daily temperature projections from CMIP6 models. Clim. Dyn., 61, 3893–3910. https://doi.org/10.1007/s00382-023-06778-8.

Lukman R., 2010. Kajian Kondisi Morfometri Dan Beberapa Parameter Stratifikasi Perairan Danau Toba. J. Limnotek, 17, 158–170.

Mamenun M., Pawitan H., Sopaheluwakan A., 2014. Validasi Dan Koreksi Data Satelit Trmm Pada Tiga Pola Hujan Di Indonesia. J. Meteorol. dan Geofis., 15. https://doi.org/10.31172/jmg.v15i1.169.

Mareta L., Agiel H.M., Hadiningrum T., 2024. Historical and projected rainfall climatology in Sumatra based on the CMIP6. IOP Conf. Ser. Earth Environ. Sci., 1359, 12089. https://doi.org/10.1088/1755-1315/1359/1/012089.

Najib M.K., Nurdiati S., 2021. Koreksi Bias Statistik Pada Data Prediksi Suhu Permukaan Air Laut Di Wilayah Indian Ocean Dipole Barat Dan Timur. Jambura Geosci. Rev., 3, 9–17. https://doi.org/10.34312/jgeosrev.v3i1.8259.

Ngai S.T., Tangang F., Juneng L., 2017. Bias correction of global and regional simulated daily precipitation and surface mean temperature over Southeast Asia using quantile mapping method. Glob. Planet. Change, 149, 79–90. https://doi.org/https://doi.org/10.1016/j.gloplacha.2016.12.009.

Noël T., Loukos H., Defrance D., Vrac M., Levavasseur G., 2021. A high-resolution downscaled CMIP5 projections dataset of essential surface climate variables over the globe coherent with the ERA5 reanalysis for climate change impact assessments. Data Br., 35, 106900. https://doi.org/10.1016/j.dib.2021.106900.

Nurdiati S., Bukhari F., Sopaheluwakan A., Septiawan P., Hutapea V., 2024. ENSO and IOD impact analysis of extreme climate condition in Papua, Indonesia, 19, 1–18. https://doi.org/10.21163/gt_2024.191.01.

Nurdiati S., Khatizah E., Najib M.K., Hidayah R.R., 2021. Analysis of rainfall patterns in Kalimantan using fast fourier transform (FFT) and empirical orthogonal function (EOF). J. Phys. Conf. Ser., 1796, 12053. https://doi.org/10.1088/1742-6596/1796/1/012053.

Nurdiati S., Sopaheluwakan A., Najib M.K., 2019. Statistical Bias Correction for Predictions of Indian Ocean Dipole Index With Quantile Mapping Approach. Int. MIPAnet Conf. Sci. Math. https://doi.org/10.31219/osf.io/7dq2j.

Nurdiati S., Sopaheluwakan A., Septiawan P., 2022. Joint Distribution Analysis of Forest Fires and Precipitation in Response to ENSO, IOD, and MJO (Study Case: Sumatra, Indonesia). Atmosphere (Basel), 13. https://doi.org/10.3390/atmos13040537.

Ona B.J., Raghavan S.V., Nguyen N.S., Ngai S.T., Nguyen T.H., 2024. Changes in Future Rainfall over Southeast Asia Using the CMIP6 Multi-model Ensemble. J. Atmos. Sci. Res., 7, 62–82. https://doi.org/10.30564/jasr.v7i2.6335.

Prasetyo B., Irwandi H., Pusparini N., 2018. Karakteristik Curah Hujan Berdasarkan Ragam Topografi Di Sumatera Utara. J. Sains Teknol. Modif. Cuaca, 19, 11. https://doi.org/10.29122/jstmc.v19i1.2787.

Rafhida S.A., Nurdiati S., Budiarti R., Najib M.K., 2024. Bias correction of lake Toba rainfall data using quantile delta mapping. Cauchy, 9, 297–309. https://doi.org/10.18860/ca.v9i2.29124.

Reboita M.S., Ferreira G.W. de S., Ribeiro J.G.M., da Rocha R.P., Rao V.B., 2023. South American Monsoon Lifecycle Projected by Statistical Downscaling with CMIP6-GCMs. Atmosphere (Basel), 14, 1380. https://doi.org/10.3390/atmos14091380.

Riahi K., van Vuuren D.P., Kriegler E., Edmonds J., O'Neill B.C., Fujimori S., Bauer N., Calvin K., Dellink R., Fricko O., Lutz W., Popp A., Cuaresma J.C., K.C.S., Leimbach M., Jiang L., Kram T., Rao S., Emmerling J., Ebi K., Hasegawa T., Havlik P., Humpenöder F., Da Silva L.A., Smith S., Stehfest E., Bosetti V., Eom J., Gernaat D., Masui T., Rogelj J., Strefler J., Drouet L., Krey V., Luderer G., Harmsen M., Takahashi K., Baumstark L., Doelman J.C., Kainuma M., Klimont Z., Marangoni G., Lotze-Campen H., Obersteiner M., Tabeau A., Tavoni M., 2017. The Shared Socioeconomic Pathways and their energy, land use, and greenhouse gas emissions implications: An overview. Glob. Environ. Chang., 42, 153–168. https://doi.org/10.1016/j.gloenvcha.2016.05.009.

Salathé E.P., 2003. Comparison of various precipitation downscaling methods for the simulation of streamflow in a rain-shadow river basin. Int. J. Climatol., 23, 887–901. https://doi.org/10.1002/joc.922.

Schoof J.T., 2015. High-resolution projections of 21st century daily precipitation for the contiguous U.S. J. Geophys. Res., 120, 3029–3042. https://doi.org/10.1002/2014JD022376.

Schoof J.T., Robeson S.M., 2016. Projecting changes in regional temperature and precipitation extremes in the United States. Weather Clim. Extrem., 11, 28–40. https://doi.org/10.1016/j.wace.2015.09.004.

Schroeter S., Bi D., Law R.M., Loughran T.F., Rashid H.A., Wang Z., 2024. Global-scale future climate projections from ACCESS model contributions to CMIP6. J. South. Hemisph. Earth Syst. Sci., 74. https://doi.org/doi.org/10.1071/ES23029.

Sihotang H., Purwanto M.Y.J., Widiatmaka W., Basuni S., 2012. Model for Water Conservation of Lake Toba. J. Nat. Resour. Environ. Manag., 2, 65–72. https://doi.org/10.19081/jpsl.2012.2.2.65.

Supharatid S., Nafung J., Aribarg T., 2022. Projected changes in temperature and precipitation over mainland Southeast Asia by CMIP6 models. J. Water Clim. Chang, 13, 337–356. https://doi.org/10.2166/wcc.2021.015.

Teutschbein C., Seibert J., 2012. Bias correction of regional climate model simulations for hydrological climate-change impact studies: Review and evaluation of different methods. J. Hydrol., 456–457, 12–29. https://doi.org/10.1016/j.jhydrol.2012.05.052.

Tukidi, 2010. Karakter Curah Hujan Di Indonesia. J. Geogr., 7, 136–145.

Voldoire, A., 2018. CNRM-CERFACS CNRM-CM6-1 model output prepared for CMIP6 CMIP. https://doi.org/10.22033/ESGF/CMIP6.1375,

Wild J., Hall J.K., 1982. Aspects of hydrology in the province of North Sumatra, Indonesia. Proc. Inst. Civ. Eng., 73, 85–108. https://doi.org/10.1680/iicep.1982.1873.

Wu T., Chu M., Dong M., Fang Y., Jie W., Li J., Li W., Liu Q., Shi X., Xin X., Yan J., Zhang F., Zhang J., Zhang L., Zhang Y., 2018. BCC BCC-CSM2MR model output prepared for CMIP6 CMIP historical. https://doi.org/10.22033/ESGF/CMIP6.2948.

Xia P., Tahara T., Kakue T., Awatsuji Y., Nishio K., Ura S., Kubota T., Matoba O., 2013. Performance comparison of bilinear interpolation, bicubic interpolation, and B-spline interpolation in parallel phase-shifting digital holography. Opt. Rev., https://doi.org/10.1007/s10043-013-0033-2.

Yukimoto S., Koshiro T., Kawai H., Oshima N., Yoshida K., Urakawa S., Tsujino H., Deushi M., Tanaka T., Hosaka M., Yoshimura H., Shindo E., Mizuta R., Ishii M., Obata A., Adachi Y., 2019. MRI MRI-ESM2.0 model output prepared for CMIP6 CMIP historical. Earth Syst. Grid Fed.